Full-Polarization 3D Metasurface Cloak with Preserved Amplitude and Phase

Yihao Yang, Liqiao Jing, Bin Zheng, Ran Hao, Wenyan Yin, Erping Li,* Costas M. Soukoulis,* and Hongsheng Chen**

Polarization, amplitude, and phase are three fundamental properties of light. When light is incident onto an object, the object will block the transmitted wave and cause scattering, rendering the object observed. An invisibility cloak can suppress the scattering fields and reconstruct the polarization, amplitude, and phase of the transmitted light as if the object did not exist. Such an invisibility cloak was nearly inconceivable until the macroscopic cloaking method of transformation optics was proposed by Pendry et al.[1] Since then, several invisibility cloak methods were experimentally demonstrated,[2–13,21,22] however, it faces a grand challenge on special polarization[2–5,8–13,21,22] or amplitude/phase distortions.[3–10,13,14] In this work, we overcame the limitations and successfully realized a full-polarization 3D carpet cloak with preserved amplitude and phase by utilizing metasurfaces,[15] which are able to control the polarization,[16] amplitude,[17] and phase of light.[18] The work made a milestone on the invisibility cloak and will have a broad range of potential applications, particularly in macroscopic object cloaking and illusions.

Practical invisibility cloaks, in people's minds, should guide light around hidden objects with preserved polarization, amplitude, and phase as if the object did not exist. Invisibility cloaks remained in the realm of science fantasy until the advent of transformation optics and metamaterials, making the realization of invisibility cloaks a scientific possibility. Tremendous progress has been made toward the realization of amplitude- or phase-preserved invisibility cloaks. Amplitude-preserved carpet cloaks can be achieved by utilizing a quasiconformal mapping technique and embedding the entire cloak into a dielectric background.[3–5,19] Phase-preserved cloaks can be obtained by eikonal approximation, i.e., keeping the refraction index unchanged and altering the impedance. A remarkable example of this method is a nonmagnetic approximation, where only the relative permittivity is changed while the relative permeability remains at unity. Thus, an optical omnidirectional cloak can be achieved by embedding metal nanowires in a dielectric material.[20] Recently, a significant step toward a cloak with both preserved amplitude and phase has been made;[12] specifically, a metamaterial was designed to fully control both the refraction index and impedance, leading to the realization of a microwave unidirectional cloak based on transformation optics without any approximation for a special polarization.

The great challenge of practical cloak design is that an invisibility cloak with perfect performance (i.e., with both the phase and amplitude preserved) is difficult to achieve for full polarization, because from a transformation optics perspective, manipulating the phase and amplitude of light for full polarization requires the simultaneous control of six constitutive parameters, i.e., ε_x, ε_y, ε_z, μ_x, μ_y, μ_z, in a Cartesian coordinate system, which is extremely complex to design and implement. The majority of experimental investigations of invisibility cloaks are restricted to special polarization,[2–5,8–13,21,22] i.e., transverse electric (TE) polarization or transverse magnetic (TM) polarization. To reduce the complexity, two remarkable efforts have been made to implement full-polarization 3D cloaks based on isotropic materials with the constitutive parameters designed based on quasiconformal mapping methods;[6,7] however, the phase of the reflected wave is not preserved well, rendering it detectable.[14] Metasurfaces provide new ways for scientists to control the polarization, amplitude, and phase of light.[15] Studies of metasurfaces highlight a promising way to design macroscopic carpet cloaks: adjusting the local reflection phase of a ground using a metasurface and thus restoring the phase of reflected beams as if the light had impinged onto a flat mirror.[21–25] Thus, metasurface-based carpet cloaks are inherently phase-preserved, and recent studies further reveal that they are perfectly amplitude-preserved if the operational incident angle is near 0°.[21] Metasurface cloaks inherit the qualities of metasurfaces and offer multiple advantages compared with traditional quasiconformal mapping-based bulky cloaks, including ultrathin thickness, light weight, the convenience of fabrication, ease of scaling up to macroscopic, applicability at any shape and size, and no lateral shift of reflected beams.[21] However, a full-polarization 3D amplitude-and-phase-preserved cloak still remains elusive.

In this study, we designed and realized for the first time a novel 3D cloak with arbitrary shape and size based on a metasurface, which are able to completely restore the polarization, amplitude, and phase of reflected light. As metasurfaces show strong abilities to control the polarization of light based on the

Dr. Y. Yang, Dr. L. Jing, Dr. B. Zheng, Prof. H. Chen
State Key Laboratory of Modern
Optical Instrumentation
The Electromagnetics Academy
Zhejiang University
Hangzhou 310027, P. R. China
E-mail: zhengbin@zju.edu.cn; hansomchen@zju.edu.cn
Dr. Y. Yang, Dr. L. Jing, Dr. B. Zheng, Prof. R. Hao,
Prof. W. Yin, Prof. E. Li, Prof. H. Chen
College of Information Science & Electronic Engineering
Zhejiang University
Hangzhou 310027, P. R. China
E-mail: liep@zju.edu.cn
Dr. Y. Yang, Prof. C. M. Soukoulis
Department of Physics and Astronomy and Ames Laboratory-U.S. DOE
Iowa State University
Ames, IA 50011, USA
E-mail: soukoulis@ameslab.gov

DOI: 10.1002/adma.201600625

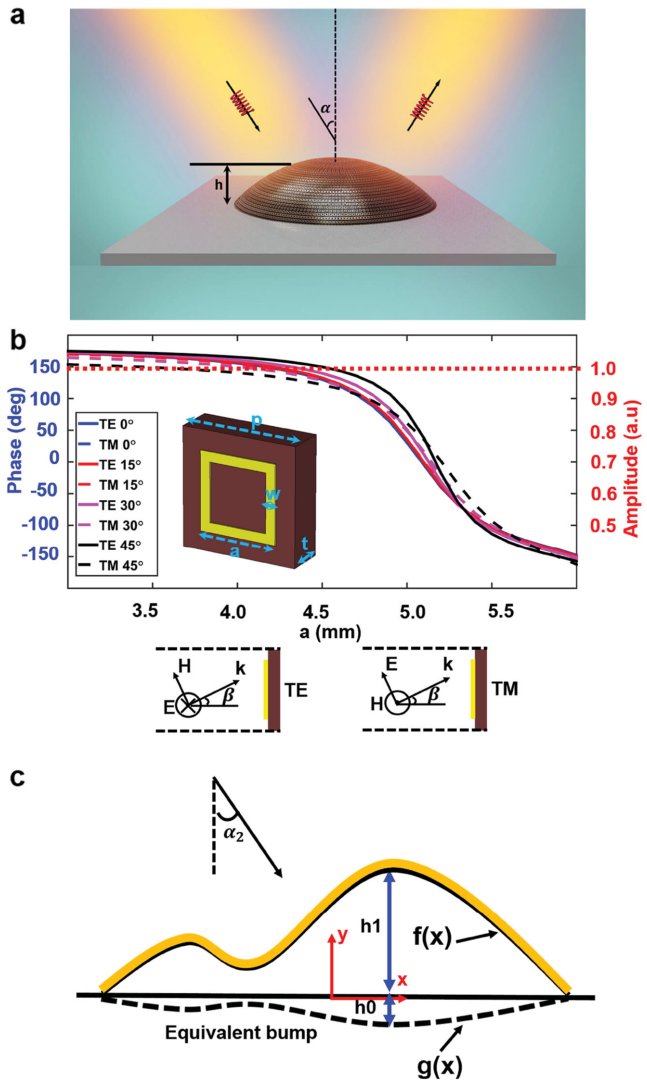

Figure 1. Scheme of a 3D metasurface cloak and unit cell design. a) Schematic view of a 3D full-polarization metasurface carpet cloak. When light with arbitrary polarization impinges onto the PEC bump, the polarization, amplitude, and phase of the reflected light will be distorted. After covering it with a gradient ultrathin metasurface, which can provide an additional phase shift to control the local reflection phase, the previously distorted reflected light will be recovered with the same polarization, amplitude, and phase as if the light impinged onto a flat mirror. b) Reflection amplitude (dotted lines) and phase (dashed lines for TM polarization and solid lines for TE polarization) of different sizes of a CRR at 7.5 GHz at an oblique incident angle of 0°, 15°, 30°, and 45°, respectively. The inset is the unit cell, where $p = 6$ mm, $w = 0.5$ mm, and $t = 2$ mm. The brown region is a substrate with a relative permittivity of 3.5 + 0.00245i. c) Equivalent bump ($g(x)$) when light is incident at an angle of α_2 onto a bump ($f(x)$) covered by a metasurface cloak (yellow region) which is formerly designed for an incident angle of α_1. Suppose that $\alpha_1 = 0°$, and $\alpha_2 = 15°$, h0 will be 0.035h1.

strong surface-confined interaction between light and subwavelength scatters and have a 2D nature, the challenge of polarization in traditional bulky invisibility cloaks can be successfully solved by designing a full-polarization metasurface cloak.

As shown in **Figure 1**a, when light impinges onto a perfect electric conductor (PEC) bump on a PEC ground with an incidence angle of α, the bump will introduce an unnecessary phase to the light, and the wavefront and polarization of the formal beams will be distorted. To compensate for these unwanted phase shifts, an ultrathin-skin metasurface consisting of many phase-shifting resonant elements will be wrapped over the bump to alter the local reflection phase at each metasurface, thus reconstructing the polarization and phase of the reflected light as if the light were incident on a flat mirror. The reflection phase induced by the metasurface cloak is denoted by

$$\delta = 180° - 2k_0 h\cos(\alpha) \quad (1)$$

where h is the height of the center point of the unit cell from the ground and k_0 is the wave vector in free space.

To ensure that our metasurface cloak works for any polarization, e.g., linear, circular or elliptical polarization, we apply a close ring resonator (CRR) with C_4 symmetry as a unit cell of the metasurface cloak,[23] as shown in Figure 1b. The CRR is on a substrate with a thickness of 2 mm, and a relative permittivity of 3.5 + 0.00245i. The thickness of our metasurface cloak is only one-nineteenth of the operational wavelength in the free space. The period of the unit cell, p, is 6 mm. When altering the size of the CRR, a, the reflection phase at 7.5 GHz will be changed, which can nearly cover the range from –180° to 180°, while the amplitude remains near unity. Because the metasurface unit cells have C_4 symmetry and are considerably smaller than the operational wavelength in the free space, when the incident angle is smaller than 45°, reflection phases for both TE (transverse electric) and TM (transverse magnetic) polarizations are very close, thus, a cloak based on this metasurface will be full-polarization. Besides, the metasurface cloak can still work well when the incident angle slightly deviates from the targeted one. As shown in Figure 1c, when light is incident on the bump with a height of $f(x)$ covered by a metasurface cloak which is formerly designed for α_1 incidence angle, at the incidence angle of α_2, the equivalent bump will be (see the Supporting Information)

$$g(x) = f(x) \times (\cos(\alpha_2) - \cos(\alpha_1))/\cos(\alpha_2) \quad (2)$$

Considering $\alpha_1 = 0°$, and $\alpha_2 = 15°$, $g(x) = -0.035 f(x)$, where the negative value indicates that the equivalent bump is a depression. Because the height of the bump is reduced by 96.5%, the scattering of the bump will dramatically decrease, and the metasurface cloak still works very well at an oblique incidence angle within 15°.

As a demonstration, full-wave simulations of a triangle metasurface cloak (see the Supporting Information for the geometry parameters of each unit cell) with a tilt angle of 24.6° and a size of 176 mm × 42 mm were performed in CST Microwave Studio, as shown in **Figure 2.** Without the metasurface cloak, strong scattering and a distorted wavefront will occur under a TE (Figure 2b) or TM (Figure 2e) plane wave at a vertical incidence. After wrapping over an ultrathin gradient metasurface cloak, the scattering fields are reconstructed with the same phase and amplitude as if the light were incident on a flat reflective ground for both the TE (Figure 2a) and TM wave (Figure 2d). In addition, from Figure 2c,f, one can see that the metasurface cloak can work well at an oblique incidence angle

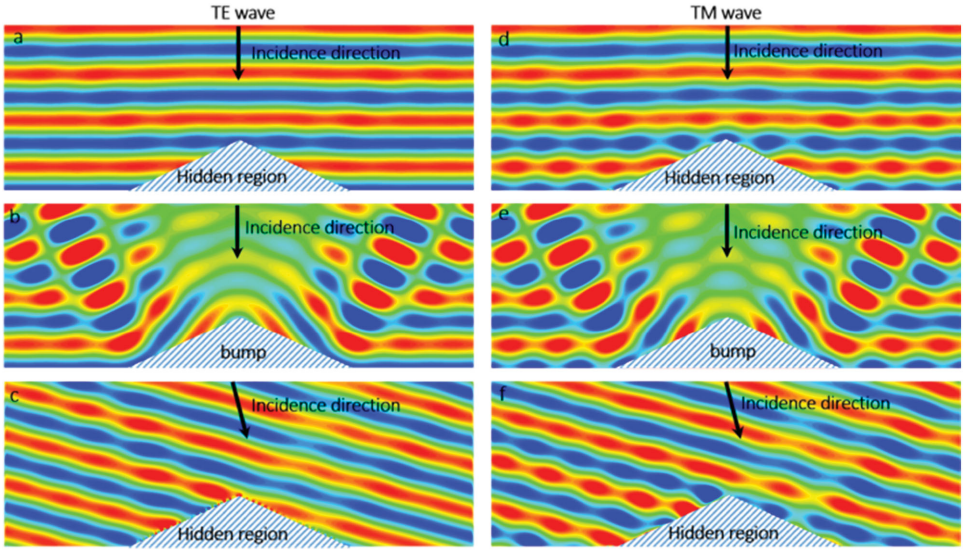

Figure 2. a–f) Full-wave simulations of a full-polarization metasurface cloak. Reflected transverse electric field distributions at 7.5 GHz when a TE plane wave is incident to a bump covered by a polarization-insensitive metasurface cloak at normal incidence a), a bare bump at normal incidence b), and a cloaked bump at an incidence angle of 15° c). Reflected transverse magnetic field distributions at 7.5 GHz when a TM plane wave is incident to a bump covered by a full-polarization metasurface cloak at normal incidence d), a bare bump at normal incidence e), and a cloaked bump at an oblique incidence angle of 15° f).

of at least 15°. This demonstrated that the cloak is free from detection by phase-sensitive instruments, as predicted in previous theoretical model. Note that an ideal metasurface cloak requires that the reflection phases change along the slope of the triangle continuously. However, in practice, because we used the metasurface unit cells, whose size is about 1/7 operational wavelength, the reflection phases of the practical structures do not change homogenously. This will cause some small wavefront distortions of the scattering field. This inhomogeneous imperfections can be reduced if the sizes of designed unit cells are much smaller than the operation wavelength.

An arbitrary-shape 3D metasurface cloak in microwave frequency has been experimentally realized, as shown in **Figure 3**c. The shape of our cloak is a pyramid without a top, the tilt angle is still 24.6°, and its size is 176 mm × 176 mm × 34 mm. In the implementation, we printed the CRR structure on a substrate, namely, a 2 mm Teflon woven glass fabric copper-clad laminate with a permittivity of 3.5 and $t_g\delta < 0.0007$ at 7.5 GHz.

In the experimental setup, a PEC bump covered with the metasurface cloak sample is put on a flat PEC ground plane. A linearly polarized Gaussian wave from the high-directivity lens antenna is incident with an azimuthal angle (θ, ϕ) onto the sample, where $\theta = 180° - \alpha$, as shown in

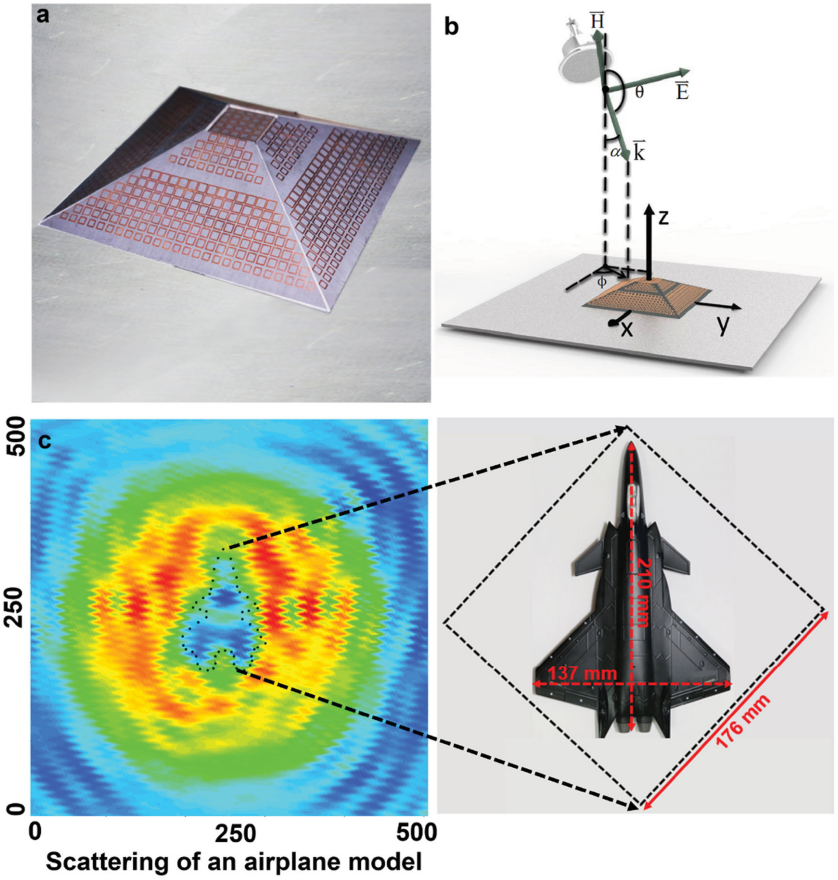

Figure 3. a) Fabricated metasurface carpet cloak. b) Measurement scheme. A linearly polarized Gaussian wave from the high-directivity lens antenna is incident with an azimuthal angle (θ, φ) onto the sample, where $\theta = 180° - \alpha$. c) Measured Hx field distributions of a metal aircraft model in z = 114 mm plane. A TE polarized wave with electric field along y direction is incident onto the aircraft model vertically.

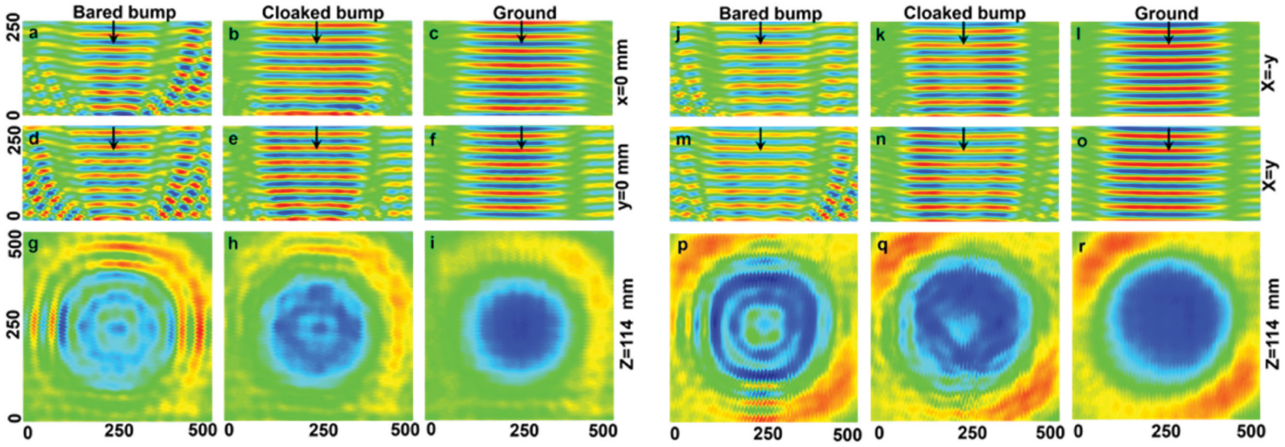

Figure 4. Case I ($\alpha = 0°$, the electric field of incident wave is along *y* direction, and the magnetic field along *x* direction is measured): a–c) Measured field distributions in the $x = 0$ mm plane for a bare bump, cloaked bump, and flat mirror, respectively. d–f) Measured field distributions in the $y = 0$ mm plane for a bare bump, cloaked bump, and flat mirror, respectively. g–i) Measured field distributions in the $z = 114$ mm plane for a bare bump, cloaked bump, and flat mirror, respectively. Case II ($\alpha = 0°$, the electric field of incident wave is along $x = -y$ direction, and the magnetic field along $x = y$ direction is measured): j–l) Measured field distributions in the $x = -y$ plane for a bare bump, cloaked bump, and flat mirror, respectively. m–o) Measured field distributions in the $x = y$ plane for a bare bump, cloaked bump, and flat mirror, respectively. p–r) Measured field distributions in the $z = 114$ mm plane for a bare bump, cloaked bump, and flat mirror, respectively. The black arrows represent the incidence direction of EM wave.

Figure 3b. Both TE (electric field is in the XY plane) and TM (magnetic field is in the XY plane) wave incidences are considered. The experimental measurements were carried out in an anechoic chamber. We measured the magnetic field distributions over the samples in three different orthogonal planes (see details in the Supporting Information). As an example, an aircraft model is used for measurement under TE wave at vertical incidence. The field patterns measured in the $z = 114$ mm plane are shown in Figure 3c, from which we can see that the aircraft model causes lots of scatterings and the measured scattering pattern well reflects the contour of the aircraft itself.

In the first case (Case I), we measured the field distributions when the wave with E_x polarization is normally incident onto the sample from the top ($\alpha = 0°$). The measured magnetic field distributions in three planes, $x = 0$ mm plane, $y = 0$ mm plane, and $z = 114$ mm plane, are shown in **Figures 4**a–c, d–f, and g–i, respectively. The cloaking frequency has shifted slightly from 7.5 GHz to 8 GHz in the implementation. Figure 4a,d,g is the measured magnetic fields in the $x = 0$ mm, $y = 0$ mm, and $z = 114$ mm planes for the bare bump, respectively. The figures show that when the EM wave impinges on the bump, the reflected beams are distorted and scattered into different directions. From the scattering field pattern shown in

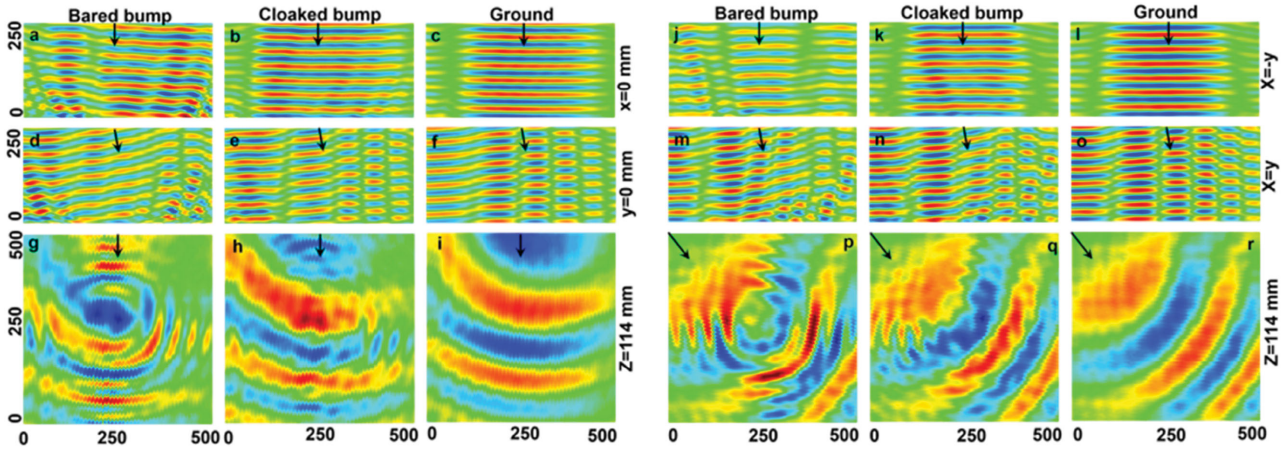

Figure 5. Case III ($\alpha = 10°$, $\phi = 0°$, the electric field of incident wave is along *y* direction (TE polarization, electric field in XY plane), and the magnetic field along *x* direction is measured): a–c) Measured results in the $x = 0$ mm plane for a bare bump, cloaked bump, and flat mirror, respectively. d–f) Measured results in the $y = 0$ mm plane for a bare bump, cloaked bump, and flat mirror, respectively. g–i) Measured results in the $z = 114$ mm plane for a bare bump, cloaked bump, and flat mirror, respectively. Case IV ($\alpha = 10°$, $\phi = 45°$, the electric field of incident wave is along $x = -y$ direction (TE polarization, electric field in XY plane), and the magnetic field along $x = y$ direction is measured): j–l) Measured field in the $x = -y$ plane for a bare bump, cloaked bump, and flat mirror, respectively. m–o) Measured field in the $x = y$ plane for a bare bump, cloaked bump, and flat mirror, respectively. p–r) Measured field in the $z = 114$ mm plane for a bare bump, cloaked bump, and flat mirror, respectively. The black arrows represent the incidence direction of EM wave.

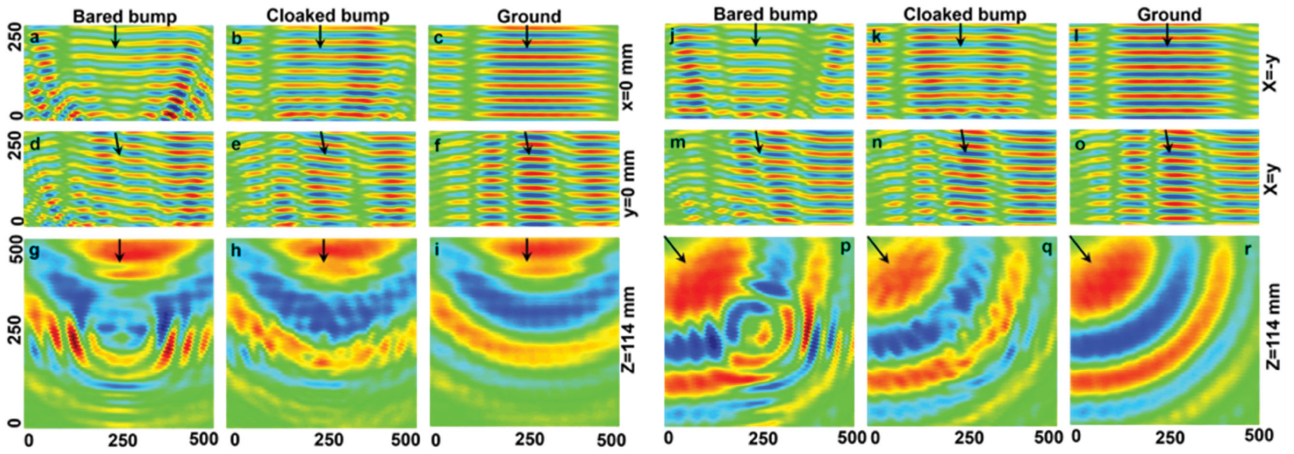

Figure 6. Case V ($\alpha = 10°$, $\phi = 0°$, the magnetic field of incident wave is along y direction (TM polarization, magnetic field in XY plane), and the magnetic field along y direction is measured): a–c) Results in the $x = 0$ mm plane for a bare bump, cloaked bump, and flat mirror, respectively. d–f) Results in the $y = 0$ mm plane for a bare bump, cloaked bump, and flat mirror, respectively. g–i) Results in the $z = 114$ mm plane for a bare bump, cloaked bump, and flat mirror, respectively. Case VI ($\alpha = 10°$, $\phi = 45°$, the magnetic field of incident wave is along $x = -y$ direction (TM polarization, magnetic field in XY plane), and the magnetic field along $x = -y$ direction is measured): j–l) Field distributions in the $x = -y$ plane for a bare bump, cloaked bump, and flat mirror, respectively. m–o) Field distributions in the $x = y$ plane for a bare bump, cloaked bump, and flat mirror, respectively. p–r) Field distributions in the $z = 114$ mm plane for a bare bump, cloaked bump, and flat mirror, respectively. The black arrows represent the incidence direction of EM wave.

Figure 4g, one can see the contour of the geometry of the bare PEC bump. While after covering it with a metasurface cloak (with the measured fields shown in Figure 4b,e,h), the distortion of the reflected phase and polarization are reconstructed, and the split beams rejoin again. One can see the measured results are very similar to those measured for the ground plane (Figure 4c,f,i).

In the second case (Case II), we keep all the setup the same with Case I, but the polarization of the electric field is along the $x = -y$ direction ($\alpha = 0°$, $\phi = 45°$). From the measured results for the bare bump (Figure 4j,m,p) metasurface cloak (Figure 4k,n,q), and flat ground plane (Figure 4l,o,r), one can see that the metasurface cloak can well cancel the scattering fields caused by the bare PEC bump.

In the next step, we measured the case when the wave is incident with an azimuthal angle of $\alpha = 10°$, $\phi = 0°$. In order to see that the cloak works for full-polarization waves, both TE (Case III) and TM (Case V) waves are measured. The results are shown in **Figure 5**a–i (TE wave with electric field along y direction) and **Figure 6**a–i (TM wave with the magnetic field along y direction), respectively. Good cloaking performance has been demonstrated from the measured magnetic field distribution in all planes, which further confirms the effectiveness of our cloak.

Finally, we measured the cases when the wave is incident with an azimuthal angle of $\alpha = 10°$, $\phi = 45°$. Similarly, both TE (Case IV) and TM (Case VI) waves are measured, the results are shown in Figure 5j–r (TE wave with electric field along $x = -y$ direction) and Figure 6j–r (TM wave with magnetic field along $x = -y$ direction), respectively. Because in a 3D space, arbitrary polarization can be created by combing TE and TM polarizations, all of the measured results prove that our metasurface cloak can completely restore the amplitude and phase for full-polarization waves.

To quantitatively measure the total scattering reduction achieved by our metasurface cloak, in the experiment, we evaluated the reduced total radar cross section (RCS) of the metasurface cloak in two typical incident planes for vertical ($\alpha = 0°$) and oblique incidence ($\alpha = 10°$, $\phi = 0°$). The reduced total RCS is defined as

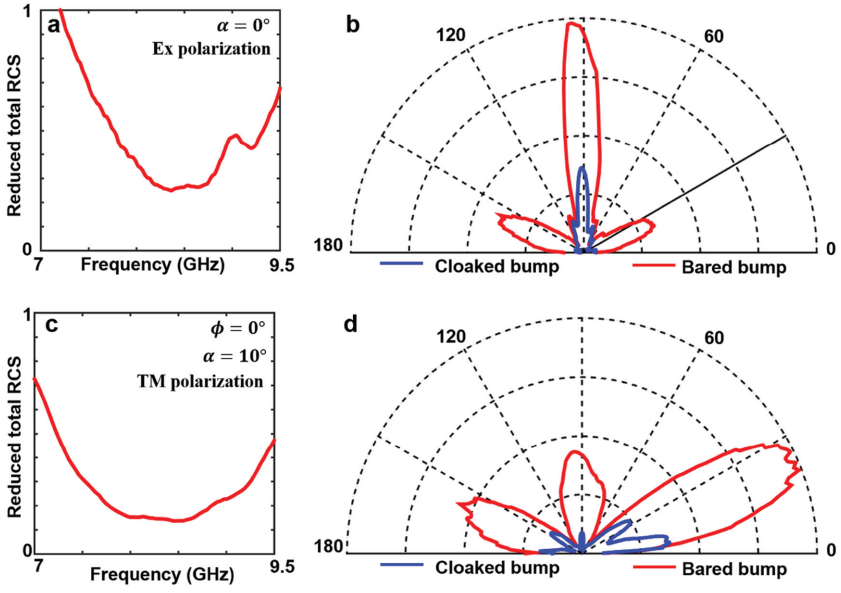

Figure 7. a,b) Measured reduced total scattering RCS, and normalized differential RCS in the $x = 0$ mm plane at 8 GHz for Case I, respectively. c,d) Measured reduced total scattering RCS, and normalized differential RCS in the $y = 0$ mm plane at 8 GHz for Case V, respectively.

$$\sigma_{\text{reduced}} = \sigma_{\text{cloaked}} / \sigma_{\text{uncloaked}} = \oint_{\Omega} (|H_{\text{cloaked,scat}}|^2 / |H_{\text{uncloaked,scat}}|^2) d\Omega \quad (3)$$

where $H_{\text{cloaked,scat}} = H_{\text{cloaked,tot}} - H_{\text{ground,tot}}$, $H_{\text{uncloaked,scat}} = H_{\text{uncloaked,tot}} - H_{\text{ground,tot}}$ $H_{\text{cloaked,tot}}$, $H_{\text{uncloaked,tot}}$, and $H_{\text{ground,tot}}$ are the total magnetic fields (all the incident waves are the same) for metasurface cloak, bare PEC bump, and flat ground, respectively. The integral spans all visible angles. The calculated reduced total RCS as a function of frequency are shown in **Figure 7**, from which, one can see that with the metasurface cloak, the total scattering dramatically decreases around 8 GHz in the experiment. The 3 dB bandwidth of the metasurface cloak is about 18.2% (7.5 GHz to 9 GHz) in the experiment. In Figure 7b,d, we show the measured differential RCS ($\sigma_{\text{diff}} = 2\pi\rho |H_{\text{scatter}}|^2$, where ρ = 250 mm, and all the incident waves are the same) at 8 GHz for vertical incidence and oblique incidence, respectively. Note that in the figures, we normalized both curves with the maximum value of the differential RCS of the bared PEC bump. One can see that the metasurface cloak can strongly suppress the scatterings for almost all of measured view angles.

In this paper, at the first time, we experimentally demonstrated a full-polarization arbitrary-shaped 3D metasurface cloak with preserved amplitude and phase in microwave frequencies. By taking the unique feature of metasurfaces, we successfully developed the novel cloak which lifts the limitations of special polarization, impedance mismatching, and lateral shift of the reflected beams in existing invisibility cloaks. Both the simulated and experimental results prove that our postulated cloak can completely restore the polarization, amplitude and phase of light for full polarization as if light was incident on a flat mirror. Though the bandwidth and operational view angle of our metasurface cloak are limited, we have pushed the implementation of a practical invisibility cloaks forward. The convenient fabrication of our cloak paves a feasible way to pursue an industrial large-scale full-polarization 3D cloak in both microwave and terahertz frequencies and may find potential applications in vehicle cloaking and illusions.

Supporting Information

Supporting Information is available from the Wiley Online Library or from the author.

Acknowledgements

This work was sponsored by the National Natural Science Foundation of China under Grant Nos. 61322501, 61275183, and 61571395, the National Program for Special Support of Top-Notch Young Professionals, the Program for New Century Excellent Talents (NCET-12-0489) in University, the Fundamental Research Funds for the Central Universities, and the Innovation Joint Research Center for Cyber-Physical-Society Systems. Work at Ames Laboratory was partially supported by the U.S. Department of Energy, Office of Basic Energy U. Science, Division of Materials Sciences and Engineering (Ames Laboratory is operated for the S. Department of Energy by Iowa State University under Contract No. DE-AC02-07CH11358).

Received: February 1, 2016
Revised: April 12, 2016
Published online: May 24, 2016

[1] J. B. Pendry, D. Schurig, D. R. Smith, *Science* **2006**, *312*, 1780.
[2] D. Schurig, J. J. Mock, B. J. Justice, S. A. Cummer, J. B. Pendry, A. F. Starr, D. R. Smith, *Science* **2006**, *314*, 977.
[3] R. Liu, C. Ji, J. J. Mock, J. Y. Chin, T. J. Cui, D. R. Smith, *Science* **2009**, *323*, 366.
[4] J. Valentine, J. Li, T. Zentgraf, G. Bartal, X. Zhang, *Nat. Mater.* **2009**, *8*, 568.
[5] L. H. Gabrielli, J. Cardenas, C. B. Poitras, M. Lipson, *Nat. Photon.* **2009**, *3*, 461.
[6] H. F. Ma, T. J. Cui, *Nat. Commun.* **2010**, *1*, 21.
[7] T. Ergin, N. Stenger, P. Brenner, J. B. Pendry, M. Wegener, *Science* **2010**, *328*, 337.
[8] B. Zhang, Y. Luo, X. Liu, G. Barbastathis, *Phys. Rev. Lett.* **2011**, *106*, 033901.
[9] X. Chen, Y. Luo, J. Zhang, K. Jiang, J. B. Pendry, S. Zhang, *Nat. Commun.* **2011**, *2*, 176.
[10] H. Chen, B. Zheng, *Sci. Rep.* **2012**, *2*, 255.
[11] D. Shin, Y. Urzhumov, Y. Jung, G. Kang, S. Baek, M. Choi, H. Park, K. Kim, D. R. Smith, *Nat. Commun.* **2012**, *2*, 1213.
[12] N. Landy, D. R. Smith, *Nat. Mater.* **2013**, *12*, 25.
[13] H. Chen, B. Zheng, L. Shen, H. Wang, X. Zhang, N. I. Zheludev, B. Zhang, *Nat. Commun.* **2013**, *4*, 3652.
[14] B. Zhang, T. Chan, B-I. Wu, *Phys. Rev. Lett.* **2010**, *104*, 233903.
[15] N. Yu, F. Capasso, *Nat. Mater.* **2014**, *13*, 139.
[16] N. Yu, F. Aieta, P. Genevet, M. A. Kats, Z. Gaburro, F. Capasso, *Nano Lett.* **2012**, *12*, 6328.
[17] C. Pfeiffer, A. Grbic, *Phys. Rev. Lett.* **2013**, *110*, 197401.
[18] N. Yu, P. Genevet, M. A. Kats, F. Aieta, J. P. Tetienne, F. Capasso, Z. Gaburro, *Science* **2011**, *334*, 333.
[19] J. Li, J. B. Pendry, *Phys. Rev. Lett.* **2008**, *101*, 203901.
[20] W. Cai, U. K. Chettiar, A. V. Kildishev, V. M. Shalaev, *Nat. Photon.* **2007**, *1*, 224.
[21] J. Zhang, Z. L. Mei, W. R. Zhang, F. Yang, T. J. Cui, *Appl. Phys. Lett.* **2013**, *103*, 151115.
[22] X. Ni, Z. J. Wong, M. Mrejen, Y. Wang, X. Zhang, *Science* **2015**, *349*, 1310.
[23] L. Y. Hsu, T. Lepetit, B. Kante, *Prog. Electromagnetics Res.* **2015**, *152*, 33.
[24] N. M. Estakhri, A. Alu, *IEEE Microw.Wireless Compon. Lett.* **2014**, *13*, 1775.
[25] B. Orazbayev, N. Mohammadi Estakhri, M. Beruete, A. Alù, *Phys. Rev. B* **2015**, *91*, 195444.